Journal of Power Sources 205 (2012) 281–289

Contents lists available at SciVerse ScienceDirect

Journal of Power Sources

journal homepage: www.elsevier.com/locate/jpowsour

Flexible power control of fuel cells using sliding mode techniques

Fernando A. Inthamoussou[a], Ricardo J. Mantz[b], Hernán De Battista[a,*]

[a] CONICET, LEICI, Facultad de Ingeniería, Universidad Nacional de La Plata, Argentina
[b] CICpBA, LEICI, Facultad de Ingeniería, Universidad Nacional de La Plata, Argentina

ARTICLE INFO

Article history:
Received 20 September 2011
Received in revised form
23 December 2011
Accepted 1 January 2012
Available online 10 January 2012

Keywords:
Fuel cells
Power control
Sliding modes
Hydrogen
Power converters

ABSTRACT

The energy conversion system considered in this work consists of a fuel cell connected to a DC-bus through a switching converter. Particularly, the paper deals with the control of the electrical variables of this system. The control problem is addressed using tools of variable structure systems theory. The dynamic behavior of the system is first analyzed. Then, sliding mode algorithms to control electrical variables according to different power management objectives are developed. Thus, different control strategies such as fuel cell voltage/current regulation, maximum power point tracking and/or load current regulation can be followed. After studying their stability properties, these algorithms are combined to achieve a globally stable control over the whole electrical operating locus of the fuel cell. Experimental results on a test circuit are presented.

1. Introduction

Fuel cell knowledge and technology are currently undergoing an impressive development, motivated in part by environmental concern [1,2]. Much research activity has been oriented to investigate the electrochemistry and some technological aspects with the goals of costs reduction and efficiency improvement [3]. On the other hand, potential applications of fuel cells ranging from low power devices (mobile phones, laptops) to high power systems (electric power stations), also deserve great interest from the research community. Another issue that is now receiving increasing attention is fuel cell control because of its prime importance in reliability and flexibility. Fuel cell control is a very challenging topic. It is hampered by dynamic complexities, intertwines between variables and subsystems, scarcity of measurable variables, perturbations and uncertainties. Many internal variables and subsystems such as temperature, hydration, pressure of gases, breathing subsystem, etc., must be controlled to avoid degradation and irreversible damages [4–7].

Fuel cell outputs, namely voltage and current between electrodes, depend on both the electrochemical reaction and the external load. Naturally, electric power flow should match the load demand. Therefore, there are essentially two ways of controlling the power extracted from the cell: controlling the electrochemical reaction or controlling the load. In the first approach, the electrochemical reaction is controlled by manipulating the feed flows. The dynamics of the electrochemical reaction taking place in the fuel cell are extremely fast. The problem is that the power control system bandwidth is limited by the dynamics of the feed, breathing, heat management, etc. Additionally, the power control loop strongly interacts with the rest of the fuel cell control system. Moreover, some conflicting control objectives may arise. The second approach consists of adjusting the load impedance effectively seen from the fuel cell terminals without the need of manipulating the electrochemical reaction [8–11]. This is performed by interfacing an electronic converter between cell and load. The fuel cell power is transferred to the load periodically by switching at high frequency the conduction state of some semiconductor devices. Converter input and output powers are ideally equal, but voltage and current are not. The impedance effectively seen from the cell terminals can therefore be modified by adjusting the duty cycle of the converter. The main advantage of this approach is that the power control dynamics are decoupled from the remaining dynamics of the fuel cell. This provides the flexibility to pursue different control objectives, namely

- Fuel cell current (or voltage) regulation.
- Load current (or voltage) regulation.
- Combined regulation capabilities.

The energy conversion system considered in this paper consists of a fuel cell connected to a DC-bus and loads through a step-down electronic converter. Attention is focused on the control of the electronic converter according to the different control objectives

* Corresponding author. Tel.: +54 221 425 9306; fax: +54 221 425 9306.
E-mail address: deba@ing.unlp.edu.ar (H. De Battista).

0378-7753/$ – see front matter © 2012 Elsevier B.V. All rights reserved.
doi:10.1016/j.jpowsour.2012.01.012

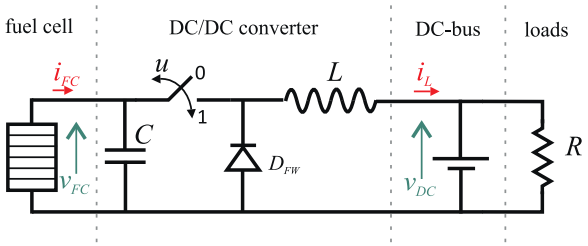

Fig. 1. Energy conversion system.

mentioned above. This task is addressed from a variable structure system (VSS) approach. A VSS is composed of various continuous subsystems with a switching logic. A particular mode of operation is achieved when switching occurs at a very high frequency, ideally infinite, constraining the system state to a sliding surface. This kind of operation is called sliding mode (SM). Its most distinctive feature is that the SM dynamics is not the average of the subsystem dynamics, they are actually completely different. Also, SM exhibits reduced-order dynamics and it is robust to parameter uncertainties and external disturbances [12]. Electronic converters and, therefore, the energy conversion system considered here fall within the definition of VSS. Furthermore, the energy conversion is performed by switching the converters topology at high frequency. Thereby, they are natural candidates to SM control. The literature and practical experience about SM control of electronic converters is vast [13]. Interestingly, the application of SM concepts to control fuel cell systems offers new problems and perspectives. This is due to the fact that the converter dynamics in fuel cell applications differ significantly with respect to conventional uses such as uninterrupted power supply. For instance, multiplicity and local unstable dynamics may appear because of nonlinearity in the fuel cell polarization curve.

Keeping this in mind, the system dynamics are first analyzed by investigating the sliding motions on natural sliding surface candidates to fulfill the control objectives. Particular attention is focused on convergence to the sliding surface, SM existence and stability conditions under control input constraints. Furthermore, algorithms combining these sliding motions are developed to achieve a more flexible and globally attractive control of the fuel cell system.

Theoretical and numerical results are validated experimentally on a test system composed of a step-down converter, a control circuit and a fuel cell emulator.

2. Energy conversion system

Fig. 1 shows a schematic diagram of the energy conversion system considered in this paper. It consists of a fuel cell, a DC/DC step-down electronic converter and a DC-bus to which different loads and sources can be connected.

2.1. Fuel cell

Fuel cell modeling is a hot research topic, and a wide variety of models, of control-oriented models to be more specific, can be found in the literature. Depending on the control objectives, models are devoted to represent the behavior of different parts of the process [6,14,15]. For instance, a pair of control-oriented models of different complexity are available for Matlab®/Simulink® users [16].[1]

[1] These models are not used here because they do not describe the current–voltage behavior over the whole operating range.

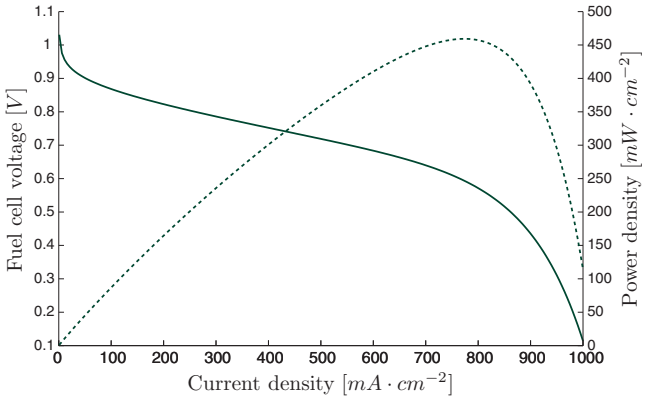

Fig. 2. Typical fuel cell polarization curve. Solid: voltage vs. current. Dashed: power vs. current.

Regarding the electrochemical behavior, it is typically modeled by means of four static equations and one dynamic equation relating electric current to partial pressures of gases. This model suffices for analysis and design of the electric power control developed in this paper. The static equations describe the reversible thermodynamic potential, the activation, ohmic over-voltage and concentration over-voltages, which lead to the following current–voltage characteristic of the fuel cell [8]

$$v = E_{oc} - i \cdot r - A \cdot \ln(i) + m \cdot \exp(n \cdot i) \tag{1}$$

where v: fuel cell potential, E_{oc}: open-circuit voltage, i: current density, r: area-specific resistance, A: slope of the Tafel line, m and n: constants in the mass-transfer over-voltage.

Thus, from the electrical terminals, the fuel cell is represented by its polarization curve, such as that plotted in Fig. 2 [3,17]. The open-circuit voltage of fuel cells is very low, around 1.2 V. Output voltage falls below this value because of different losses. At low current level, voltage drop is caused by activation losses. Ohmic losses predominate in the linear part of the curve. At high current level, voltage falls abruptly because of the reduction in gas exchange efficiency (gas transport losses).

Conversion efficiency (η) is a very important issue in fuel cell operation and control. It is usually defined as the ratio of output power to fuel input. Since fuel consumption is proportional to current density, conversion efficiency increases linearly with fuel cell potential v and decreases with current density i [18]. For a given power demand, efficiency can be improved, for instance, increasing the air flow rate and pressure. From this point of view, the fuel cell should be operated to the greater possible air flow rate and pressure. However, if the compressor power consumption is considered, an optimal combination of these variables can be obtained for each load current [19,4].

The polarization curve exhibits a maximum, called maximum power point (MPP), that lies in the transition between the ohmic and concentration regions. At this point, the cell is operated with its maximum power capacity. Then, for a given power demand below MPP, there are two possible operating points located at both sides of the MPP. The desired operating locus is the portion of the polarization curve located to the left of the MPP, where efficiency is higher. Within this region there is an operating point that is optimum in terms of economics, i.e. taking also capital costs into account.

Several fuel cells are usually connected in series to increase output voltage and then in parallel to gain in power capacity. The static relationship between voltage and current of the fuel cell stack is denoted here as

$$v_{FC} = f_{FC}(i_{FC}) \tag{2}$$

Naturally, the graphical representation of f_{FC} on the plane (v_{FC}, i_{FC}) has the same shape as the polarization curve of the individual fuel cells (Fig. 2).

2.2. Electronic converter: steady-state analysis

The electronic converter consists of a capacitor C, an inductor L, an electronic switch S_W and a free wheel diode D_{FW}. The capacitor and inductor are the input and output storage devices, respectively. The electronic switch performs the energy transfer from input to output. The free wheel diode provides a path to the inductor current when the switch is off. In this application, a fuel cell stack is connected to the converter input whereas the converter output is connected to a DC-bus. DC-bus voltage is imposed by a battery pack or a large capacitor. Here, the purpose of the DC-bus is to provide the peak power demands, so that the fuel cell does not need to be oversized.

In normal operation, converter switching occurs at very high frequency. Then, an average model of the switch can be used to perform a steady-state analysis of the converter dynamics. A key role in this analysis is played by the duty cycle of the converter (δ), defined as the fraction of time that the switch is on. By definition, $0 < \delta < 1$. In steady state, input and output variables are constant and related via the duty cycle. In fact, it is quite easy to infer that

$$i_{FC} = \delta \cdot i_L \tag{3}$$

Neglecting losses, input and output powers are equal, i.e. $i_{FC} v_{FC} = i_L v_{DC}$. Then, it follows that

$$v_{DC} = \delta \cdot v_{FC} \tag{4}$$

Output voltage is lower than input voltage in steady state, hence the name step-down converter. In turn, input current is lower than output current. Then, the impedance effectively seen from the fuel cell terminals is higher than the load impedance. The operating point of the cell moves along the polarization curve as δ is varied. It is convenient to design the system so that the DC-bus voltage is lower than the MPP voltage of the fuel cell. Thus, the fuel cell can be controlled all along its desired operating locus.

2.3. System dynamics

The above analysis is valid in steady state. The average model can still be used to investigate the slow dynamics of the converter as well as to control it using δ as control variable. However, much more efficient control algorithms, for instance SM control, can be designed from an instantaneous model of the switch.

The structure and dynamics of the system change dramatically with the switch position. When the switch is on, the resulting LC circuit exhibits an oscillatory second-order dynamics. Conversely, when the switch is off, two isolated circuits with first-order dynamics arise. Let u be a discrete variable representing the switch position, i.e. $u = 1$ when the switch is on, and $u = 0$ otherwise. Dynamics of both converter structures can be combined into a single second-order model:

$$\begin{cases} \dot{i}_{FC} &= \dfrac{1}{C f'_{FC}(i_{FC})}(i_{FC} - i_L u) \\ \dot{i}_L &= \dfrac{1}{L}(f_{FC}(i_{FC})u - v_{DC}) \\ u &\in \{0, 1\} \end{cases} \tag{5}$$

where f'_{FC} is the derivative of f_{FC} with respect to i_{FC}.

Trajectories on the state plane, for both switch positions, can be obtained numerically after eliminating the time variable in (5). Fig. 3 depicts the state portraits. When the switch is off, the fuel cell current decreases as the input capacitor charges up to the open-circuit voltage of the fuel cell. Meanwhile, the load current vanishes linearly. Both switch and diode are unidirectional, meaning that load current cannot be reversed. Thus, all trajectories converge to the origin $P_0 = (0, 0)$. On the other hand, when the switch is on, the state trajectories are damped spirals centered at the point $P_1 = (f_{FC}^{-1}(v_{DC}), f_{FC}^{-1}(v_{DC}))$. Again, neither load current nor fuel cell current nor capacitor voltage can be negative because of unidirectionality of switch and diodes.

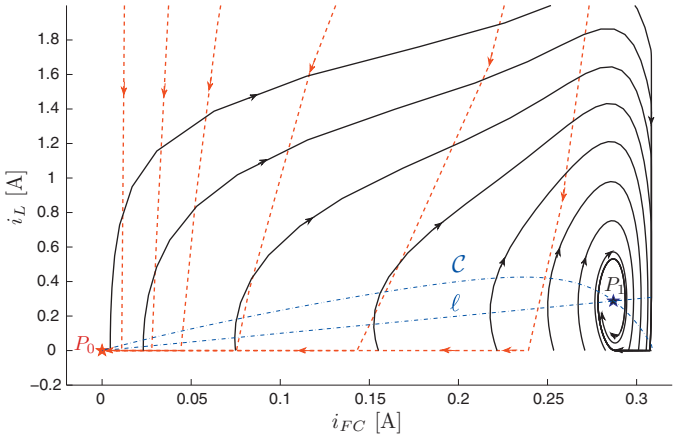

Fig. 3. State portrait for both positions of the switch (solid: $u = 1$, dashed: $u = 0$).

Remark: For the sake of clarity, the mathematical model (5) neglects switch and diode nonlinearities. Nevertheless, they are taken into account when plotting the state trajectories in Fig. 3 and when investigating the convergence properties of the control algorithms in the next section.

Remark: The dashed line labeled with $\mathcal{C}$ in Fig. 3 depicts the power curve of the fuel cell normalized by the DC-bus voltage. This curve characterizes the power balance locus of the electronic converter ($i_L v_{DC} = i_{FC} v_{FC}$).

3. Sliding mode control

3.1. Background on sliding mode

Let us consider a scalar switched system of the form

$$\begin{cases} \dot{x} = f(x) + g(x)u \\ y = h(x) \end{cases} \tag{6}$$

where $h(x)$ is an output of relative degree equal to 1, i.e. $\langle \nabla h, g \rangle \neq 0$ with ∇h being the gradient of $h(x)$. Furthermore, suppose without loss of generality that $\langle \nabla h, g \rangle < 0$. Let the switching law be:

$$u = sign(h) := \begin{cases} 1 & \text{if } h > 0 \\ 0 & \text{otherwise} \end{cases} \tag{7}$$

Suppose that, as a result of this switching law, the reaching condition

$$h \cdot \dot{h} < 0 \tag{8}$$

locally holds around the manifold $\mathcal{S} = \{x \mid h(x) = 0\}$. That is, all state trajectories originated close enough to $\mathcal{S}$ will locally point toward it. Then, the control action will switch at (ideally) infinite frequency as the state trajectory crosses the manifold in both directions. This particular mode of operation is called sliding regime or sliding mode. For obvious reasons, SM is a powerful approach for analysis and design of electronic circuits commanded by switches [20,13]. Among other attractive features, SM exhibits robust properties and reduces the order of the system dynamics [12]. Note that the output of the system ($h(x)$) is set to zero, i.e. no dynamics are present in the output evolution once the sliding regime is established. Moreover,

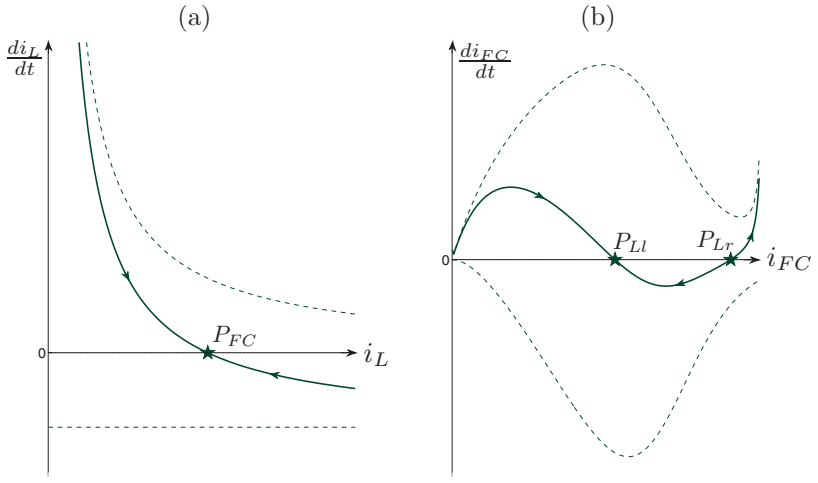

Fig. 4. Sliding dynamics for (a) fuel cell and (b) load current regulation.

zero regulation error is maintained despite all kinds of disturbances provided the reaching condition (8) holds. Therefore, the SM dynamics coincide with the zero-dynamics. Hence, a minimum phase behavior is needed to obtain stable sliding motions.

From the surface invariance conditions $h = 0$ and $\dot{h} = 0$, a fictitious smooth equivalent control action can be defined [12]:

$$u_{eq}(x) = -\frac{\langle \nabla h, f \rangle}{\langle \nabla h, g \rangle}. \tag{9}$$

By replacing u in (6) with (9), the SM dynamics is obtained. A necessary condition for u_{eq} to be well-defined is that the system has a relative degree equal to one. The necessary and sufficient condition (8) for SM existence can be written in terms of the equivalent control as follows:

$$0 < u_{eq}(x) < 1. \tag{10}$$

Actually, a VSS comprises another mode of operation: the reaching mode (RM). When there are no restrictions on the control effort, a continuous control action can be designed to reach the sliding surface with a prescribed reaching dynamics. However, the convergence of all state trajectories to the surface is, generally, not assured for bounded inputs. Sometimes, several changes of structure may occur before the sliding regime is finally established. In this paper we investigate the domain of attraction of the proposed sliding surfaces and the sliding domains, i.e. the regions of the sliding surfaces where SM exists.

In real applications, switching frequency is deliberately bounded to avoid undesirable effects and losses. A simple method consists in incorporating hysteresis to the switching law. A constant-amplitude ripple on the controlled output is therefore obtained whereas the switching frequency is kept bounded.

The dynamical model (5) of the fuel cell system under consideration takes the affine form (6), where $x = [\, i_{FC} \quad i_L \,]^T$ is the system state and u denotes the switch position taking discrete values $\{0, 1\}$. On the normal operating region of the system (i.e. for $i_L > 0$, $i_{FC} > 0$ and $v_{FC} > 0$), the drift and controlled vector fields are

$$f(x) = \begin{bmatrix} \frac{i_{FC}}{Cf'_{FC}} \\ \frac{-v_{DC}}{L} \end{bmatrix} \qquad g(x) = \begin{bmatrix} \frac{-i_L}{Cf'_{FC}} \\ \frac{f_{FC}(i_{FC})}{L} \end{bmatrix}.$$

The controlled vector field $g(x)$ has its two components different from zero on the normal operating region. Hence, both the fuel cell and load currents are relative-degree-one outputs of the dynamical model. Then, any of these variables can be set to a reference value through an SM control. Next, we investigate the local SM existence and the global convergence properties. In particular, the domains of attraction of the sliding surfaces, and of the stable equilibrium points, are discussed.

Hereinafter, some control objectives are considered which can be fulfilled by different sliding mode control loops.

3.2. Fuel cell current regulation

The first control objective consists in regulating the fuel cell current to a reference value. The fuel cell voltage or power can be regulated in a similar fashion because of the static relationship between them through the function f_{FC}. This way, the operating point of the fuel cell can be adjusted. For instance, the fuel cell can be controlled to operate at its nominal point or at the MPP.

This control goal can be achieved by establishing a sliding regime on a fuel cell current dependent switching surface. A natural sliding surface candidate is

$$\mathcal{S}_{FC} = \{x | h_{FC} = i_{FC}^{ref} - i_{FC} = 0\} \tag{11}$$

The sliding function h_{FC} satisfies the transversality condition $\langle \nabla h_{FC}, g \rangle < 0$. From the invariance condition ($h_{FC} = 0, \dot{h}_{FC} = 0$), the equivalent control yields:

$$u_{eq_{FC}} = \frac{i_{FC}^{ref}}{i_L} \tag{12}$$

Then, according to (9), the sliding domain is

$$\mathcal{D}_{FC} = \{x \in \mathcal{S}_{FC} | i_L > i_{FC}\} \tag{13}$$

In other words, sliding mode exists on the sliding surface just above the line $\ell = \{x | i_L - i_{FC} = 0\}$ drawn in Fig. 3.

The first-order SM dynamics is determined by replacing u in (5) with (12):

$$\dot{i}_L = \frac{-v_{DC}}{L} + \frac{f_{FC}(i_{FC}^{ref}) i_{FC}^{ref}}{L i_L} \tag{14}$$

Fig. 4a plots this equation on the plane $(i_L, \dot{i}_L)$ where a single and stable equilibrium point P_{FC} can be identified. This point is the intersection between the sliding surface $\mathcal{S}_{FC}$ and the normalized fuel cell power curve $\mathcal{C}$. Its coordinates are $P_{FC} = (i_{FC}^{ref}, (f_{FC}(i_{FC}^{ref}) i_{FC}^{ref} / v_{DC}))$. Two situations may arise. First, P_{FC} belongs to the sliding domain $\mathcal{D}_{FC}$. In this case, the state converges asymptotically to it by sliding on $\mathcal{S}_{FC}$. Second, P_{FC} does not belong to $\mathcal{D}_{FC}$, i.e. it is located below the line ℓ. So, the state slides on $\mathcal{S}_{FC}$ until leaving the surface when

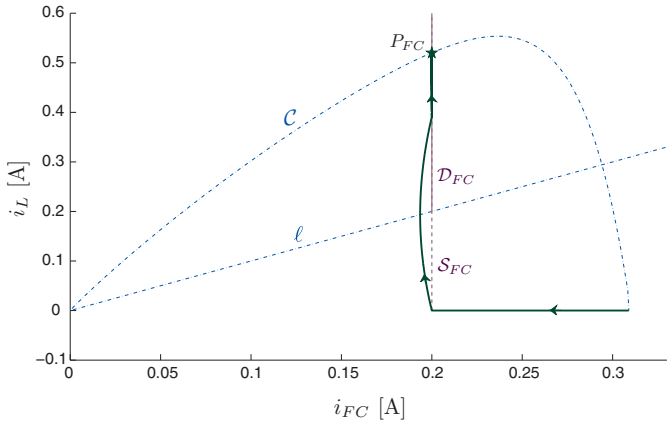

Fig. 5. State trajectory for SM fuel cell current regulation (converter initially at rest).

the SM existence condition is violated. Consequently, fuel cell current control makes sense only for current references $i_{FC}^{ref} < f_{FC}^{-1}(v_{DC})$ that also satisfy the step-down condition $v_{DC} < v_{FC}$. Note that this result is independent of the control algorithm, but inherent to the converter restrictions.

Remark: Since curve $\mathcal{C}$ is the power balance locus of the system, all possible equilibrium points necessarily lie on this curve, particularly between P_0 and P_1.

The existence condition investigated above is only local. However, it can be inferred from the state portrait of Fig. 3 that convergence to the sliding surface is global. On the one hand, all trajectories originating from the right of the surface point toward it because fuel cell current decreases with time when $u = 0$ (recall the first equation of (5)). All trajectories originating from the left of the surface and above line ℓ also point to the surface. In fact, the fuel cell current increases as $u = 1$ and $i_L > i_{FC}$. Conversely, trajectories from the left of the surface and below line ℓ do not point toward the surface (that is why SM does not exist below ℓ). In any event, the state evolves upwards and crosses ℓ, finally reaching the surface in finite time.

Fig. 5 shows the state trajectory when the fuel cell is connected to the converter initially at rest and controlled to regulate the input current (i_{FC}) at a constant value. The sliding surface and its sliding domain are plotted with dashed and solid lines, respectively. Fig. 6 displays the corresponding time evolution of currents and voltages. Notice that the sliding regime is not established the first time the state trajectory reaches the surface because that point does not belong to the sliding domain. In fact, the surface is crossed causing the undershoot in Fig. 6a. However, sliding mode exists from the second time the surface is reached. During SM, the fuel cell current

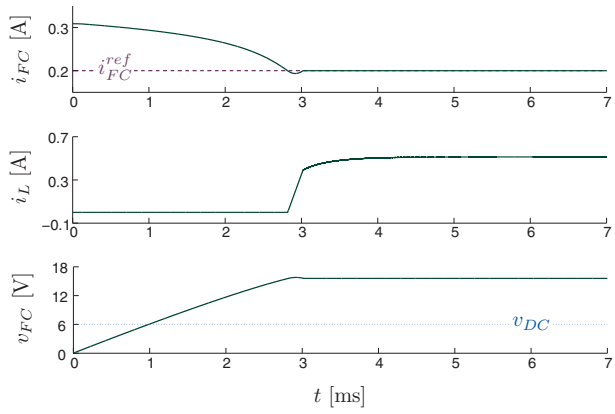

Fig. 6. Time response for SM fuel cell current regulation (converter initially at rest).

is kept constant at its reference value. That is, the first-order sliding dynamics is observed in the inductor current but hidden from the output variable (in this case i_{FC}). This is an interesting feature of the sliding mode approach.

3.3. Load current regulation

Now, a different control objective is considered, which consists in controlling the current (power) supplied to the load. Thus, the fuel cell system is operated as a controlled current source. This can be achieved by means of sliding mode control of the inductor current i_L. The analysis and design procedure are similar to the fuel cell current control case. First of all, we corroborate that the line

$$\mathcal{S}_L = \{x | h_L = i_L^{ref} - i_L = 0\} \tag{15}$$

qualifies as a sliding surface. In fact, the transversality condition is $(-v_{FC}/L) < 0$. The equivalent control in this case is:

$$v_{eqL} = \frac{v_{DC}}{v_{FC}} \tag{16}$$

Therefore, the sliding domain results $0 < v_{DC} < v_{FC}$, which in terms of the state variables is

$$\mathcal{D}_L = \{x \in \mathcal{S}_L | i_{FC} < f_{FC}^{-1}(v_{DC})\} \tag{17}$$

In other words, a sliding mode exists on the sliding surface to the left of the x-coordinate of P_1.

The first-order SM dynamics is determined by replacing u in (5) with (16):

$$\dot{i}_{FC} = \frac{1}{C f_{FC}(i_{FC}) f'_{FC}(i_{FC})} \left(i_{FC} f_{FC}(i_{FC}) - i_L^{ref} v_{DC} \right) \tag{18}$$

Eq. (18) may exhibit two, one or zero equilibrium points, depending on the reference current. The equilibrium points are characterized by the power balance $i_{FC} v_{FC} = i_L v_{DC}$. So, if the load power demand $i_L v_{DC}$ is higher than the maximum power that can be produced by the fuel cell (at the MPP), then no equilibrium point exists and an unstable sliding mode occurs. Conversely, if the load power demand is lower than the power limit of the fuel cell, then two equilibrium points arise. They are placed on curve $\mathcal{C}$ at both sides of the maximum power point.

Fig. 4b illustrates this situation on the plane $(i_{FC}, \dot{i}_{FC})$. It indicates that the leftmost point P_{Ll} is stable, whereas the rightmost point P_{Lr} is unstable. Because of the presence of multiple equilibria on the sliding domain, global attraction cannot be guaranteed. The domain of attraction can be determined from the state portrait. All trajectories reaching the sliding surface to the left of the unstable equilibrium (P_{Lr}) will evolve toward the stable one (P_{Ll}). So, by solving the inverse response from P_{Lr} for $u = 0$ and $u = 1$, the boundary of the domain of attraction can be computed. In Fig. 7, this boundary is labeled with $\partial\mathcal{D}_{\mathcal{A}}$ and the region to the left is the domain of attraction of P_{Ll}. The sliding surface and its corresponding sliding domain are the horizontal dashed line and the superimposed solid line, respectively.

Fig. 7 also illustrates a pair of state trajectories for initial conditions inside and outside the domain of stability. From the leftmost initial condition, the state evolves toward the surface where a stable sliding regime is established. Once in SM, the output (inductor) current is kept constant whereas the fuel cell current evolves asymptotically toward its steady state value. Fig. 8 shows the time response of currents and voltages for the stable behavior.

On the other hand, when the converter is initially at rest ($i_L = 0$, $v_{FC} = 0$), the state trajectory reaches the sliding surface to the left of P_1 but to the right of the unstable point P_{Lr}. That is, the sliding domain is reached, but an unstable sliding regime is established. Therefore, the SM cannot be sustained as input voltage v_{FC} falls below the output voltage (v_{DC}). Since then, the sliding surface is

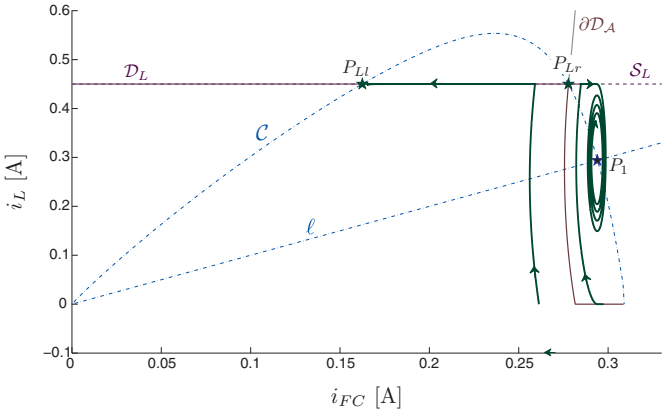

Fig. 7. State trajectories for SM load current regulation.

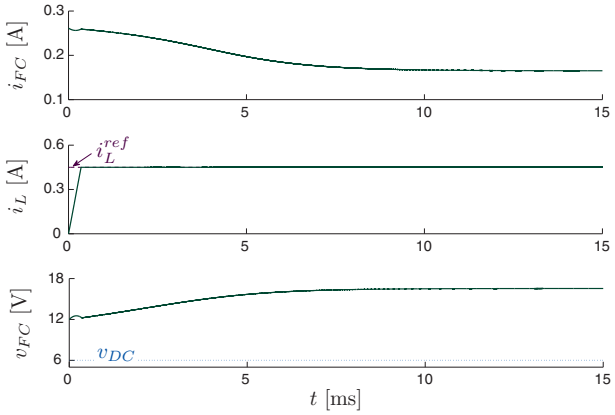

Fig. 8. Time response from an initial condition inside the stability domain.

abandoned, the switch keeps closed ($u = 1$), and the state trajectory evolves oscillatory toward the undesired equilibrium P_1. The corresponding time responses are depicted in Fig. 9.

3.4. Combined current regulation

For some designs and load demands, the stability domain of the previous output current regulation strategy may cover all the region of interest. However, this is not always the case as was illustrated in Fig. 7. In spite of that, undesirable responses can be avoided with little effort by implementing additional switching logic. For instance, global convergence can be guaranteed by

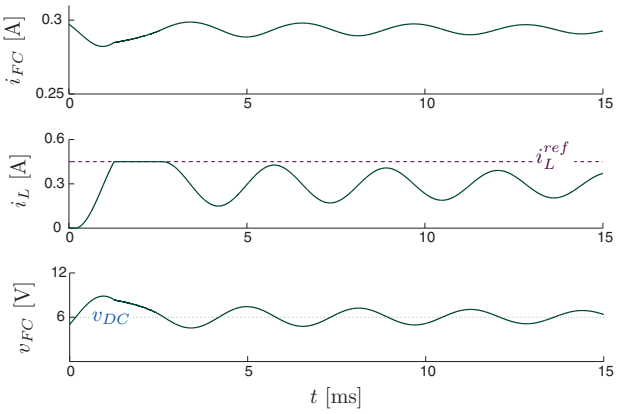

Fig. 9. Time response from an initial condition outside the stability domain.

combining the sliding surface $\mathcal{S}_L$ (15) with the sliding surface $\mathcal{S}_{FC}$ (see (11)) to attract the state trajectories originated outside the domain of attraction of P_{Ll}. This situation is illustrated in Fig. 10a. Note in particular that the previous unstable trajectory now converges to the desired equilibrium P_L. Global convergence is actually achieved. Furthermore, it is not difficult to infer that global convergence is achieved even when the output power reference exceeds the maximum deliverable power. Now being the equilibrium point at the intersection of the curve $\mathcal{C}$ with the surface $\mathcal{S}_{FC}$. This situation is illustrated in Fig. 10b.

4. Results and discussion

4.1. Experimental set-up

The proposed control strategies have been implemented on a test circuit comprised of a 4 W fuel cell emulator, a DC/DC step-down converter and a 6 V battery. The fuel cell emulator uses a PC and a real-time data acquisition board. The PC runs the fuel cell model in Matlab®/Simulink® environment. The DAQ provides the input to the model running in the PC and handles its output. This model output commands a linear current amplifier that works as a power supply for a DC/DC converter. A block diagram is depicted in Fig. 11.

Fig. 12 shows the implemented converter and controller. At the bottom, there is a picture of the power converter prototype. It is a 10 W DC/DC step-down converter using an IRFZ44N MOSFET transistor as the switch device, 1N5822 schottky diodes, an $L = 5$ mHy inductor and a $C = 470\,\mu$F capacitor. Two MAX4080 current

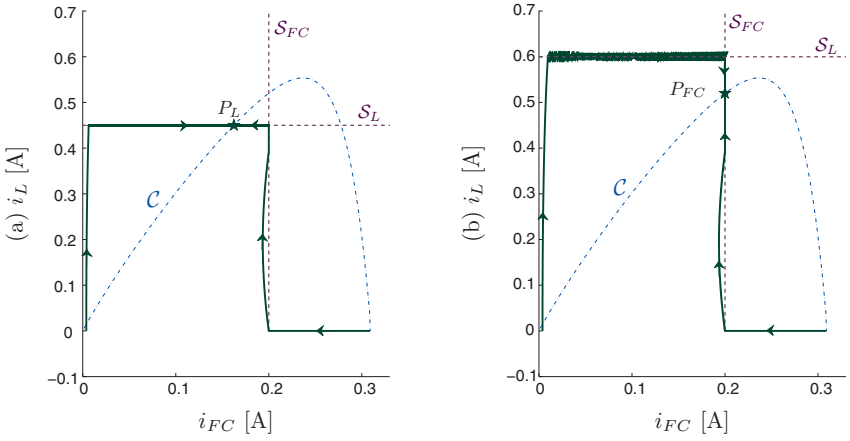

Fig. 10. State trajectories for combined SM fuel cell and load current regulation.

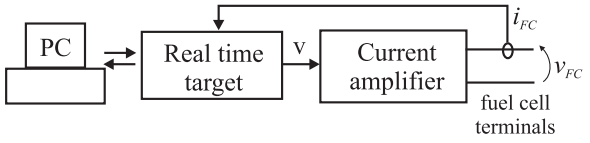

Fig. 11. Fuel cell emulator.

sensors are used to measure the converter input and output currents, whereas a voltage divider is constructed to sense voltage. Filters for the measured signals are also included. The switching transistor is driven by an isolated high frequency triggering circuit (on the left of Fig. 12). Two Schmitt-triggers, one for each current sliding mode control, were constructed using TLV3501 high-speed comparators. They provide the switching signal as a function of the corresponding current error, where their hysteresis bands are designed to limit switching frequency below 40 kHz. An ADuc841 micro controller is also available to enhance the control functionalities of the analog circuitry, for MPP tracking, supervision, monitoring, etc., and can be seen in the circuit in the upper-right portion of Fig. 12.

4.2. Experimental results

In the first experiment the operating point of the fuel cell was changed from a point of high power capacity to a point of higher efficiency. Initially, the reference was $i_{FC}^{ref} = 210$ mA and the system switched around the sliding surface (11). At $t = 0$ the set-point was changed to $i_{FC}^{ref} = 115$ mA. Fig. 13 shows the time response of the controlled current over a 200 ms time window and the state trajectory on the state space. The transistor switched off immediately after the reference step in order to reach the new sliding surface. Once it was reached, a sliding regime was established around it, so that the system state evolved within the hysteresis band designed to properly bound the switching frequency. During sliding mode, the fuel cell current was effectively regulated at its desired value despite model uncertainties. Note in the zoomed-out plot the fast response of the control system.

In the second experiment the controller was aimed at regulating the load current at $i_L^{ref} = 280$ mA, that corresponded to a 1.7 W power supply. Initially, the system was in steady state and the transistor was in conduction state. That is, the fuel cell was connected to the DC-bus and the DC load current was zero. At $t = 0$ s, the controller was activated. The transistor switched off to charge

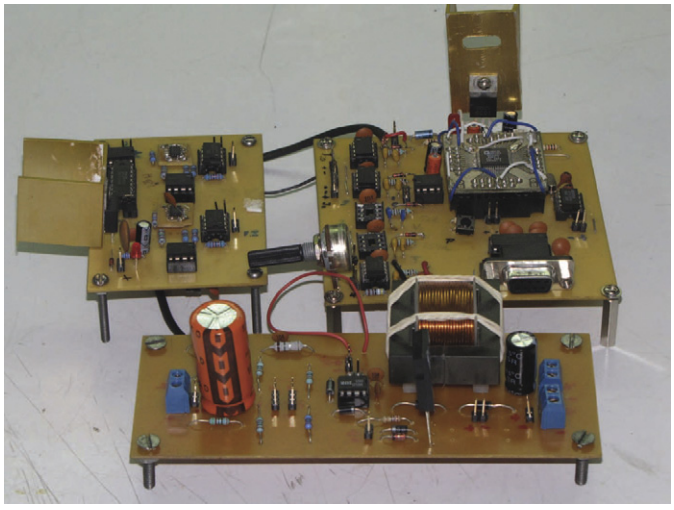

Fig. 12. DC/DC converter and control circuits.

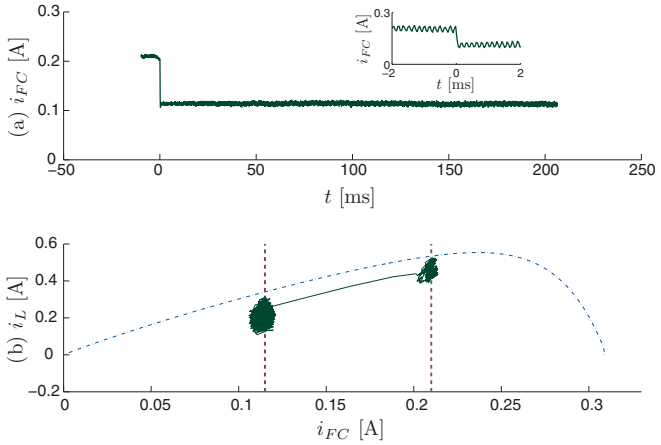

Fig. 13. Experimental results for SM fuel cell current regulation: (a) time response, and (b) state trajectory.

the inductor until the reference current was reached. Immediately after that, transistor commuted at fast frequency constraining the inductor current within a hysteresis band. Meanwhile, the fuel cell current evolved with the hidden sliding dynamics toward its steady state value. Note that there was no need of implementing a combined sliding controller since the initial condition belonged to the stability domain $\mathcal{D}_{\mathcal{A}}$ (Figs. 13 and 14).

4.3. Other results

Further results are presented here, which have been obtained by numerical simulation using the toolboxes of Simulink®. The parameters of the fuel cell used in simulations were $P_N = 1.25$ kW, $V_N = 24$ V, $I_N = 52$ A, $\eta_N = 46\%$. The converter parameters were $L = 0.3$ mHy, $C = 2000$ μF and $E = 12$ V.

4.3.1. Maximum power point tracking

Since the MPP may not be precisely known and varies with non-electrical variables, it is often convenient to implement a robust control strategy for its tracking. Based on the previous fuel cell current regulation method, an MPP tracking was developed.

The reference current to the sliding mode controller (see (11)) is provided by an outer loop that periodically updates the reference as a function of the fuel cell power deviations. Fig. 15 displays the flow chart of the proposed updating algorithm, which is based on the perturb and observe technique. Basically, this method consists in producing a small perturbation to the reference value and then

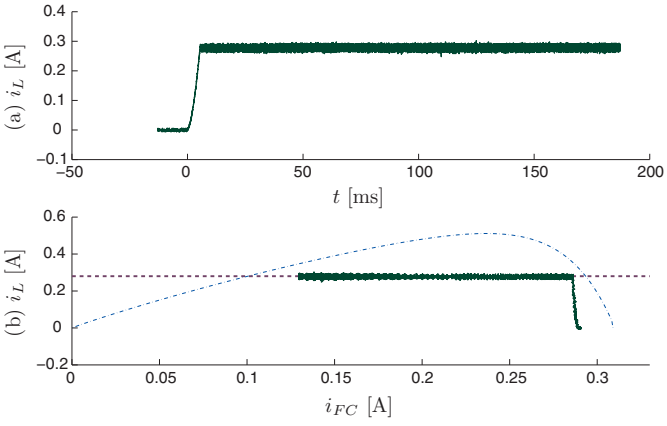

Fig. 14. Experimental results for SM load current regulation: (a) time response, (b) state trajectory.

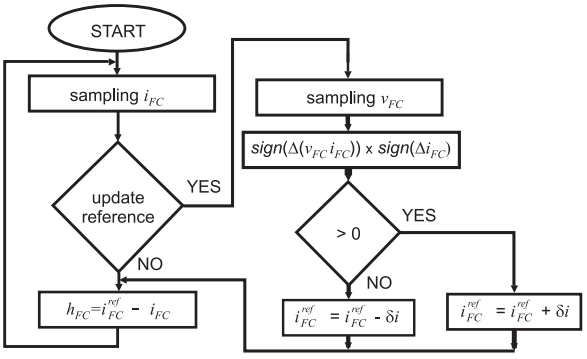

Fig. 15. MPP tracking algorithm.

observe what happens with the output power. If it increases after the perturbation, then a further perturbation in the same direction is produced, otherwise the reference is perturbed in the opposite direction. To avoid interactions, the outer loop should be much slower than the inner one.

Fig. 16 shows the time response of the MPP tracking algorithm. The fuel cell was initially regulated at its nominal point (24 V, 52 A). The algorithm run from $t = 5$ ms, periodically updating the current reference. Reference current was updated every 1 ms, and the reference step was 3 A, whereas the switching frequency was limited to 40 kHz by means of a hysteresis band around the sliding surface. At $t = 20$ ms, the MPP was reached.

The use of a sliding control as proposed here has a very important advantage: the reference fuel cell current is reached in finite time rather than asymptotically. An upper-bound for this convergence time can be derived from model (5). Furthermore, fuel cell power is kept constant – as current is – during sliding mode. Then, provided the updating time is higher than the convergence time from one sliding surface to the next, the inner and outer control loops do not interact at all.

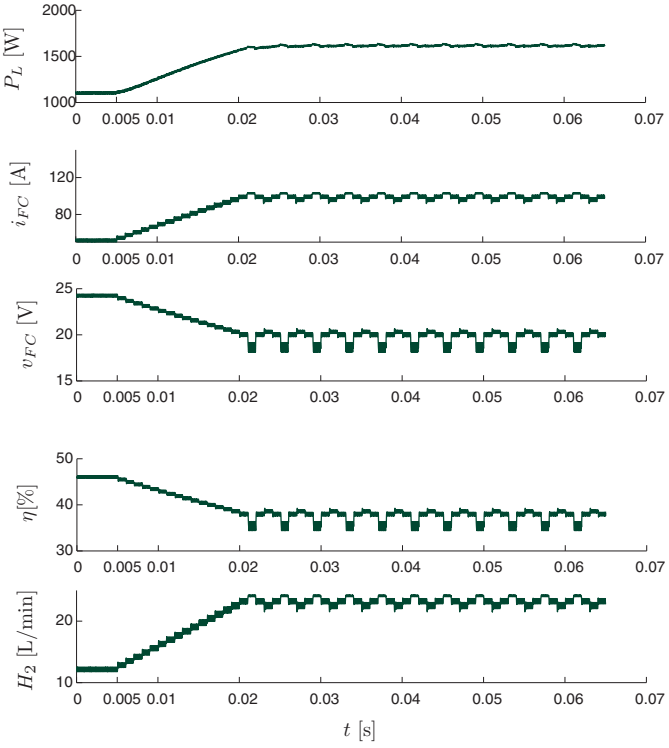

Fig. 16. Time response of the MPP tracking control.

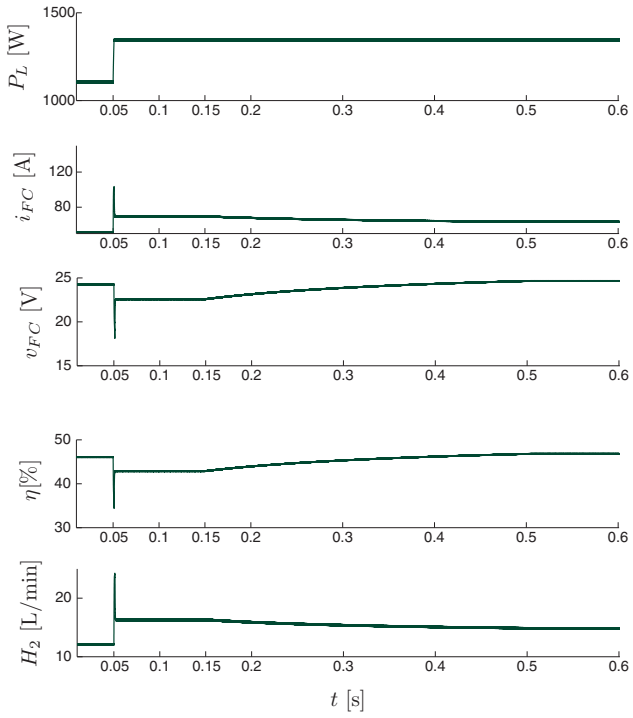

Fig. 17. Time response of the load tracking control (and air pressure control).

4.3.2. Time-varying power demand tracking

In this case, the SM load current control tracked a stepped power demand, whereas a slower feedback loop adjusted the motor compressor voltage to keep efficiency close to its nominal value.

Fig. 17 shows the time response of the control system. The fuel cell operated initially under nominal conditions. At $t = 50$ ms, a step in the power demand occurred. The SM load current controller reacted immediately, reaching the new set-point extremely fast. Fig. 18 shows how the operating point of the fuel cell, initially at q_1, moved along the polarization curve rightwards, increasing current and fuel consumption, whereas efficiency and voltage dropped. After a transient, the new operating point q_2 was reached. At $t = 150$ ms, the compressor controller was activated, increasing the air flow pressure. The fuel cell, with a much slower dynamic response than the load current one, converged to the operating point q_3 on the polarization curve that corresponded to the final air pressure p_2^0. At this point, efficiency was similar to the nominal one and higher than that obtained at q_2. It is interesting to remark that the SM load current controller was completely insensitive to the fuel cell dynamics.

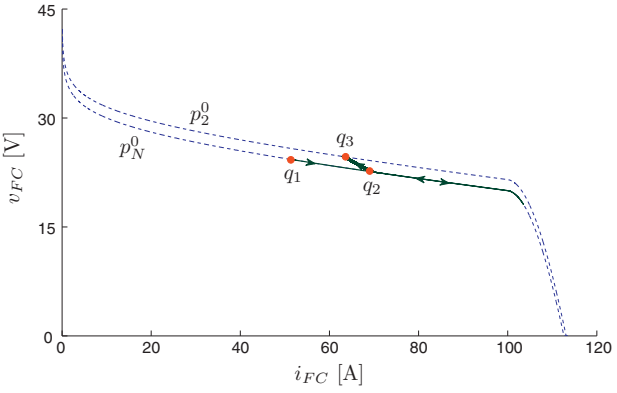

Fig. 18. Trajectory of the fuel cell operating point during load tracking control.

4.4. Discussion

Figs. 13a and 14a confirm the fast response of the SM algorithms to changes in the corresponding current set-point, whereas Figs. 13b and 14b put in evidence the strong robustness of the algorithms to model uncertainties. In fact, fuel cell (Fig. 13) and load (Fig. 14) currents were successfully regulated at their desired values despite poor regulation of the DC-bus voltage (that raised with the input power), and voltage drops and losses in the converter devices (recall that the design of the 10 W converter prototype did not take losses into account). These uncertainties explain the mismatches between the real (steady state) operating points and the theoretical ones on the polarization curve. However, these uncertainties were completely rejected by the SM controllers.

The implementation of the proposed sliding mode current controllers was extremely simple and low cost. Excellent dynamic response and robustness properties were achieved. These features make the current controllers particularly attractive to implement MPP or optimum efficiency tracking algorithms as those presented in the previous section. Figs. 16 and 17 show that the SM controller was insensitive to the dynamic response of other loops in the control system.

The proposed SM controller approach exhibits significative advantages with respect to open-loop control, that will not be able to reject disturbances, and to classical control tools like PID. On the one hand, PID implementation is more complicated that SM one because a pulse width modulator is required to convert the continuous controller output into a switching logic. There are also problems inherent to differentiation of a noisy signal and wind-up caused by input constraints, which may require careful filtering and anti-windup compensation. Tuning of the PID controller to achieve a satisfactory dynamic response, that will be of third order, is not immediate because of nonlinearity of the polarization curve. On the other hand, SM implementation and tuning is very simple, and zero steady state error in the controlled variables is achieved after a very fast transient response.

5. Conclusions

The use of sliding mode theory provides tools for designing very simple control algorithms for fuel cell systems. It is shown in the paper that SM controllers for input or output current regulation are carried out with single loop feedback configuration, making the transient response very fast and simplifying the stability analysis. Furthermore, the SM controllers can be easily combined, resulting in simple switching logics, in order to improve the performance of the individual sliding regimes. Thus, global stability is accomplished. Because of its strong stability and robustness properties, the proposed SM current control is suitable to take part of more complex control systems. The main features of the SM controllers are validated through numerical and experimental results.

Acknowledgments

We thank Prof. Jerónimo Moré for sharing with us his experience in fuel cell technology and Prof. Christopher Young for helping us with the presentation of our work.

This work was funded by the National University of La Plata (Project 11-I127), ANPCyT (PICT2007-00535), CICpBA and CONICET (PIP112-200801-01052) of Argentina.

References

[1] J. Turner, Science 285 (1999) 687–689.
[2] S. Chalk, J. Miller, Journal of Power Sources 159 (1) (2006) 73–80.
[3] J. Larminie, A. Dicks, Fuel Cell Systems Explained, 2nd ed., John Wiley & Sons Ltd., 2003.
[4] J. Pukrushpan, A. Stefanopoulou, H. Peng, Control of Fuel Cell Power Systems, Springer, 2004.
[5] C. Kunusch, A. Husar, P. Puleston, M. Mayosky, J. Moré, International Journal of Hydrogen Energy 33 (13) (2008) 3581–3587.
[6] Y. Zhang, B. Zhou, Journal of Power Sources 196 (20) (2011) 8413–8423.
[7] A. Sendjaja, V. Kariwala, IEEE Transactions on Industrial Informatics 7 (2) (2011) 163–170.
[8] Z. Zhong, H. Huo, X. Zhu, G. Cao, Y. Ren, Journal of Power Sources 176 (1) (2008) 259–269.
[9] F. Zenith, S. Skogestad, Journal of Process Control 17 (4) (2007) 333–347.
[10] A. Kirubakaran, S. Jain, R. Nema, Renewable and Sustainable Energy Reviews 13 (9) (2009) 2430–2440.
[11] N. Bizon, Applied Energy 88 (7) (2011) 2559–2573.
[12] V. Utkin, J. Guldner, J. Shi, Sliding Mode Control in Electromechanical Systems, 1st ed., Taylor & Francis, London, 1999.
[13] H. Sira-Ramírez, International Journal of Control 76 (9–10) (2003).
[14] M. Ceraolo, C. Miulli, A. Pozio, Journal of Power Sources 113 (1) (2003) 131–144.
[15] F. Zenith, F. Seland, O.E. Kongstein, B. Børresen, R. Tunold, S. Skogestad, Journal of Power Sources 162 (1) (2006) 215–227.
[16] C. Spiegel, PEM Fuel Cell Modeling and Simulation using MATLAB, Elsevier, 2008.
[17] C. Kunusch, P. Puleston, M. Mayosky, J. Moré, International Journal of Hydrogen Energy 35 (11) (2010) 5876–5881.
[18] M. Pandian, M. Anwari, B. Husodo, A. Hiendro, IPEC, 2010 Conference Proceedings, 2010, pp. 875–880, ISSN 1947-1262.
[19] D. Friedman, R. Moore, Proceedings of Electrochemical Society 27, 1998, pp. 407–423.
[20] V. Utkin, IEEE Transactions on Industrial Electronics 40 (1) (1993) 23–36.